Enhancing Conformal Prediction via Class Similarity

Ariel Fargion
Bar-Ilan University, Israel
arielfar77@gmail.com

Lahav Dabah
Bar-Ilan University, Israel
lahavdabah@gmail.com

Tom Tirer
Bar-Ilan University, Israel
tirer.tom@gmail.com

Abstract

Conformal Prediction (CP) has emerged as a powerful statistical framework for high-stakes classification applications. Instead of predicting a single class, CP generates a prediction set, guaranteed to include the true label with a pre-specified probability. The performance of different CP methods is typically assessed by their average prediction set size. In setups where the classes can be partitioned into semantic groups, e.g., diseases that require similar treatment, users can benefit from prediction sets that are not only small on average, but also contain a small number of semantically different groups. This paper begins by addressing this problem and ultimately offers a widely applicable tool for boosting any CP method on any dataset. First, given a class partition, we propose augmenting the CP score function with a term that penalizes predictions with "out-of-group" errors. We theoretically analyze this strategy and prove its advantages for group-related metrics. Surprisingly, we show mathematically that, for common class partitions, it can also reduce the average set size of any CP score function. Our analysis reveals the class similarity factors behind this improvement and motivates us to propose a model-specific variant, which does not require any human semantic partition and can further reduce the prediction set size. Finally, we present an extensive empirical study, encompassing prominent CP methods, multiple models, and several datasets, which demonstrates that our class-similarity-based approach consistently enhances CP methods.

1. Introduction

Conformal Prediction (CP) [23, 24] has emerged as a powerful statistical framework for high-stakes classification applications, such as medical diagnoses [12] and autonomous vehicle decision-making [13]. Rather than predicting a single label, the CP framework outputs a set of candidate labels with a formal guarantee of marginal coverage: under exchangeability of the calibration and test samples, the prediction set will include the correct label with a user-specified

probability. This property makes CP particularly valuable in safety-critical domains, where missing the correct label can have severe consequences. A key metric for comparing different CP methods is the average size of their prediction sets, commonly referred to in the literature as *efficiency* [2, 4, 10, 18].

In many practical scenarios, classes can be grouped into semantic categories, and users can benefit from prediction sets that are not only small on average but also contain semantically similar classes. For example, consider a medical imaging application where a classifier needs to recognize diseases. A classifier that mostly outputs prediction sets with diseases that require similar treatment, is expected to be more practically useful than one that does not, given that both have the same coverage rate and efficiency. However, while current CP approaches ensure that the true label is included in the prediction set with the pre-specified probability, they do not account for the semantic coherence of labels within the prediction set.

This paper addresses this gap and extends beyond it, ultimately offering a general tool for improving the efficiency of any CP method on any dataset. First, assuming a known partition of classes into groups, we propose augmenting the CP score function with a binary regularization term that penalizes predictions with "out-of-group" errors. We provide a theoretical analysis of this strategy and prove that it reduces the expected number of unique groups appearing in a prediction set. Interestingly, our theory also reveals a surprising property: for common class partitions, applying this penalty can simultaneously decrease the average prediction set size, regardless of the underlying CP score function. Our analysis further identifies the class similarity factors behind this improvement.

Motivated by these insights, we extend our approach and propose a model-specific variant, *which does not require any human semantic partition*. Specifically, we construct a class similarity matrix from the classifier's embedding vectors, leveraging the model's own perception of similar classes. This enables regularization that can further reduce the prediction set size and does not require any external knowledge of class groups, making it applicable for general
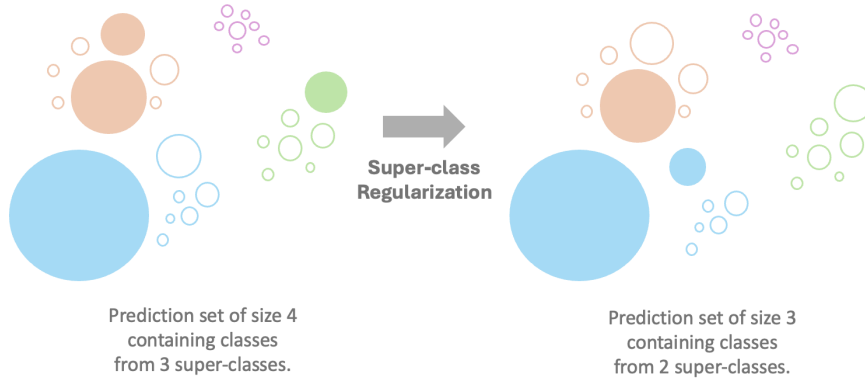
Figure 1. Illustration of prediction sets for an example before and after applying our proposed regularization. Each circle corresponds to a class, with colors indicating superclasses. Filled circles denote classes included in the prediction set, and circle size reflects the softmax value. In this example, the prediction set size decreases from 4 to 3, and the number of superclasses represented decreases from 3 to 2. We show that our regularization reduces the average prediction set size, regardless of the baseline score function.

datasets.

Finally, we present an extensive empirical study evaluating the performance of both variants, the one that uses a known, Model-Agnostic (MA), class partition, and the one that relies on Model-Specific (MS) class similarities. Our experiments encompass multiple datasets, models, and prominent CP score functions: LAC [18], RAPS [2], and SAPS [10]. We show that our class-similarity-based approach consistently enhances each of these diverse CP methods, providing a flexible and widely applicable tool for improving both the coherence and efficiency of prediction sets. To the best of our knowledge, no previous post-training approach has consistently outperformed the standard LAC in terms of average prediction set size.

Our contributions. Our main contributions can be summarized as follows.

- We propose an "out-of-group" penalty approach, independent of the original CP score function, which improves both the semantic coherence of prediction sets and their average size.
- We provide a theoretical analysis of the proposed binary penalty, proving not only its effectiveness in reducing the expected number of unique groups in the prediction set but also its non-intuitive ability to decrease the average set size for any score function.
- We introduce a model-specific variant for the approach, which further reduces the prediction set size and does not require any known class structure.
- We conduct an extensive empirical evaluation across multiple dataset-model pairs, demonstrating that both our model-agnostic and model-specific variants consistently enhance prominent CP methods, outperforming their original versions in both semantic coherence and size of their prediction sets.

2. Related Work

Clustered and group-conditional coverage CP. Several works [3, 6, 22] aim to improve coverage across heterogeneous label groups. These methods typically apply the CP procedure separately within each group, or cluster classes based on model scores, yielding prediction sets that have better group conditional coverage but larger prediction set size than their baselines.

Hierarchical and structured CP. Other works incorporate a known label hierarchy, such as a directed acyclic graph, into the conformal prediction framework. [9] and [26] share the objective of controlling the specificity of prediction sets (e.g., the number of leaf labels) alongside efficiency. [14] introduce the notion of representation complexity, defined as the minimum number of nodes whose descendants cover the prediction set, and study its trade-off with efficiency.

Hierarchical selective classification. When a hierarchical structure of labels is available, with classes located at the leaves, Goren et al. [7] extend the conformal prediction framework to achieve hierarchical selective coverage. Their approach identifies a predicted node by starting from the predicted class (which is a leaf) and ascending the hierarchy until a conformal threshold is met, in a manner similar to the APS procedure [17]. This method focuses on controlling the trade-off between predictive accuracy and the specificity of the hierarchical prediction.

Summary. To our knowledge, no prior work directly addresses the objective of improving semantic coherence within prediction sets without compromising CP efficiency, let alone leveraging class structure to *improve* efficiency. Existing works in clustered, group-conditional, and hierarchical CP focus on coverage within known groups or on rel-

atively uncommon notions of structure. Importantly, these approaches typically yield prediction sets that are larger than the baselines. In contrast, our approach reduces the number of semantically distinct groups, decreases the average set size, and is applicable across datasets and CP score functions. Moreover, our model-specific approach does not require any prior knowledge of class structure.

3. Preliminaries on Conformal Prediction

Let us present notations that are used in the paper, followed by some preliminaries on CP. We consider a C-classes classification task of the data (X, Y) distributed on $\mathcal{X} \times [C]$, where $[C] := \{1, \ldots, C\}$. The task is addressed by a classifier model (e.g., a trained deep neural network) that for each input sample $x \in \mathcal{X}$ produces a post-softmax probability vector $\hat{\pi}(x) \in \mathbb{R}^C$. The predicted class is given by $\hat{y}(x) = \arg\max_i \hat{\pi}_i(x)$.

Conformal Prediction (CP) is a methodology for reliable classification, independent of the data distribution. Given a black-box classifier, predefined $\alpha \in (0, 1)$, and a sample X, it generates a *prediction set* of classes, $\mathcal{C}(X)$, such that $Y \in \mathcal{C}_\alpha(X)$ with probability $1 - \alpha$, where Y is the true class associated with X [15, 23, 24]. The decision rule is based on a calibration set of labeled samples $\{x_i, y_i\}_{i=1}^n$. The only assumption in CP is that the random variables associated with the calibration set and the test samples are exchangeable (e.g., the samples are i.i.d.).

Let us state the general process of conformal prediction given the calibration set $\{x_i, y_i\}_{i=1}^n$ and its deployment for a new (test) sample x_{n+1} (for which y_{n+1} is unknown), as presented in [1]:
1. Define a heuristic score function $s(x, y) \in \mathbb{R}$ based on some output of the model. A higher score should encode a lower level of agreement between x and y.
2. Compute $\hat{q}$ as the $\lceil (n + 1)(1 - \alpha) \rceil / n$ quantile of the scores $\{s(x_1, y_1), \ldots, s(x_n, y_n)\}$.
3. At deployment, create the prediction set of a test sample as $\mathcal{C}(x_{n+1}) = \{y : s(x_{n+1}, y) \leq \hat{q}\}$.
CP methods possess the following coverage guarantee.

Theorem 3.1 (Theorem 1 in [1]). *Suppose that* $\{(X_i, Y_i)\}_{i=1}^n$ *and* (X_{n+1}, Y_{n+1}) *are i.i.d., and define* $\hat{q}$ *as in step 2 above and* $\mathcal{C}_\alpha(X_{n+1})$ *as in step 3 above. Then,* $\mathbb{P}(Y_{n+1} \in \mathcal{C}(X_{n+1})) \geq 1 - \alpha$.

The proof of this result is based on [23]. A proof of an upper bound of $1 - \alpha + 1/(n + 1)$ also exists. Note that the coverage is marginal: the probability is taken over the entire distribution of (X, Y) and there is no guarantee per value of X_{n+1}.

Different CP methods typically differ by their choice of score function $s(x, y)$, and a key property that they are judged according to is their average prediction set size, $\mathbb{E}[|\mathcal{C}(X)|]$, often refers to as *efficiency*.

4. Enhancing CP Using Class Similarity

In this section, we explore the properties of CP when utilizing a known partition of the C classes into G groups. Let $g : [C] \rightarrow [G]$ denote the map of classes to groups. Namely, $g(y) \in [G]$ is the index of the group that contains class $y \in [C]$.

As discussed in Section 1, we assume that the groups are superclasses with some semantic meaning. For example, the classes may be cities and the superclasses are geographical location, or the classes are types of diseases and the superclasses group those that require a similar treatment. In this case, it is reasonable for a user to prefer $\mathcal{C}(X)$ whose classes belong only to a few groups, or ideally just to the group of the true label Y.

Motivated by the above, let us set a "distance function" between classes based on their groups. Specifically, we consider the binary penalty function given by:

$$d(y, y') := \mathbb{I}\{g(y) \neq g(y')\}, \tag{1}$$

where $\mathbb{I}\{\cdot\}$ is the indicator function. That is, $d(y, y') = 0$ if y and y' belong to the same group, and otherwise $d(y, y') = 1$. For brevity, we omit the explicit dependence of $d(y, y')$ on g.

Given a sample x, all common CP methods preserve the ranking of the softmax vector $\hat{\pi}(x)$ and, in particular, include the estimated class $\hat{y}(x)$ in the prediction set before including any other class. Therefore, to reduce the number of groups in $\mathcal{C}(X)$ we propose to penalize a given score function $s(x, y)$ by $d(y, \hat{y}(x))$:

$$s_\lambda(x, y) := s(x, y) + \lambda d(y, \hat{y}(x)), \tag{2}$$

where $\lambda > 0$ is a parameter. In words, the score of a candidate y that is "semantically far" from $\hat{y}(x)$ is penalized by a value of λ.

We turn to theoretically explore the properties of CP with $s_\lambda(x, y)$. Let us denote by $\hat{q}_\lambda$ and $\mathcal{C}_\lambda(x)$ the CP threshold and prediction set when using $\lambda > 0$.

The coverage property is maintained. This follows directly from Theorem 3.1, as s_λ is a valid score that preserves the exchangeability of the calibration and test samples.

The number of out-of-group labels in the prediction set cannot increase. To show that adding the penalty term to the score cannot increase the number of classes in $\mathcal{C}_\lambda(x)$ whose group is not $g(\hat{y}(x))$, we first establish the following lemma on the relation between $\hat{q}_\lambda$ and $\hat{q}$.

Lemma 4.1. *We have* $\hat{q} \leq \hat{q}_\lambda \leq \hat{q} + \lambda$.

Proof. For *any* (x_i, y_i) in the calibration set we have $s(x_i, y_i) \leq s_\lambda(x_i, y_i) \leq s(x_i, y_i) + \lambda$. The $(1 - \alpha)$ empirical quantile for $\{s(x_i, y_i)\}$ is $\hat{q}$ and for $\{s(x_i, y_i) + \lambda\}$ is $\hat{q} + \lambda$. Therefore the $(1 - \alpha)$ empirical quantile for $\{s_\lambda(x_i, y_i)\}$ is in $[\hat{q}, \hat{q} + \lambda]$. $\square$

We now present our result on the inclusion of out-of-group labels in the prediction set.

Proposition 4.2. *Let $\mathcal{Y}_1(x) := \{y : d(y, \hat{y}(x)) \neq 0\}$. For any x and $\lambda > 0$ we have*

$$\mathcal{C}_\lambda(x) \cap \mathcal{Y}_1(x) \subseteq \mathcal{C}(x) \cap \mathcal{Y}_1(x).$$

Proof. For any $y \in \mathcal{Y}_1(x)$, we have $d(y, \hat{y}(x)) = 1$, so the inclusion in $\mathcal{C}_\lambda(x)$ implies satisfying $s(x, y) + \lambda \leq \hat{q}_\lambda \leq \hat{q} + \lambda$, where the second inequality follows from Lemma 4.1. Therefore, $s(x, y) \leq \hat{q}$, which implies $y \in \mathcal{C}(x)$. □

The proposition shows that the penalization cannot add any "far"/group-mismatched labels (w.r.t. $\hat{y}(x)$) that weren't already in the unpenalized CP; it can only remove them. This property naturally translates to decreasing the distance-weighted size. Specifically, define $S_\lambda(x) := \sum_{y=1}^{C} d(y, \hat{y}(x)) \mathbb{I}\{y \in \mathcal{C}_\lambda(x)\}$. We have $S_\lambda(x) \leq S_0(x)$ for any x, and thus also $\mathbb{E}[S_\lambda(X)] \leq \mathbb{E}[S_0(X)]$. Similarly, eliminating the pathological case of empty $\mathcal{C}(x)$, the number of groups cannot increase, as shown in the following corollary.

Corollary 4.3. *Let $\mathcal{G}_\lambda(x)$ and $\mathcal{G}(x)$ denote the groups represented in $\mathcal{C}_\lambda(x)$ and $\mathcal{C}(x)$, respectively. For any x such that $\hat{y}(x) \in \mathcal{C}(x)$ and $\lambda > 0$ we have $G_\lambda(x) \subseteq G(x)$.*

Proof. Formally, $\mathcal{G}_\lambda(x) = \{g(y) : y \in \mathcal{C}_\lambda(x)\}$ and $\mathcal{G}(x) = \{g(y) : y \in \mathcal{C}(x)\}$. We already have in Proposition 4.2 that any y with $g(y) \neq g(\hat{y}(x))$ cannot be added to $\mathcal{C}_\lambda(x)$. The assumption that $\hat{y}(x) \in \mathcal{C}(x)$ eliminates the pathological case that $s_\lambda(x, \hat{y}(x)) \leq \hat{q}_\lambda$ but $s(x, \hat{y}(x)) > \hat{q}$. So, $g(\hat{y}(x))$ is already in both $\mathcal{G}_\lambda(x)$ and $\mathcal{G}(x)$. □

Since the corollary holds for any x, it reflects the relation $\mathbb{E}[|\mathcal{G}_\lambda(X)|] \leq \mathbb{E}[|\mathcal{G}(X)|]$. This theory supports the empirical observation (in Section 6) that the empirical expectations obey $\hat{\mathbb{E}}[|\mathcal{G}_\lambda(X)|] < \hat{\mathbb{E}}[|\mathcal{G}(X)|]$, with a substantial margin.

Surprising behavior: The average prediction set size also decreases in practice. As will be shown in our experiments, with well-tuned λ (small enough), we observe $\hat{\mathbb{E}}[|\mathcal{C}_\lambda(X)|] < \hat{\mathbb{E}}[|\mathcal{C}(X)|]$, in benchmark settings, even though the penalty does not imply it directly. Actually, while we reached a guarantee for decreasing the number of "out-of-group" labels, potentially, there can be an increase in "in-group" labels, since $\hat{q} \leq \hat{q}_\lambda$ but the score of y from the same group of $\hat{y}(x)$ remains the same.

We turn to establish a theory for reduction in the average prediction set size for small enough λ. To this end, let us start by some definitions.

Definition 4.4. *Given a sample x, we have the following definitions:*

1. *"In-group" classes: $\mathcal{Y}_0(x) := \{y : d(y, \hat{y}(x)) = 0\}$ and $n_0(x) := |\mathcal{Y}_0(x)|$.*
2. *"Out-of-group" classes: $\mathcal{Y}_1(x) := \{y : d(y, \hat{y}(x)) \neq 0\}$ and $n_1(x) := |\mathcal{Y}_1(x)|$.*
3. *Per-x conditional quasi-CDF:[1] for $z \in \{0, 1\}$, $\hat{F}_z^x(t) := \frac{1}{n_z(x)} \sum_{y \in \mathcal{Y}_z(x)} \mathbb{I}\{s(x, y) \leq t\}$.*

We also make the following definitions related to the marginal distribution:

4. *Average number of "in-group" classes: $\overline{n}_0 := \mathbb{E}[n_0(X)]$.*
5. *Average number of "out-of-group" classes: $\overline{n}_1 := \mathbb{E}[n_1(X)]$.*
6. *Probability of "in-group" true label: $p_0 = \mathbb{P}(Y \in \mathcal{Y}_0(X))$.*
7. *Probability of "out-of-group" true label: $p_1 = \mathbb{P}(Y \in \mathcal{Y}_1(X)) = 1 - p_0$.*
8. *Conditional CDFs: for $z \in \{0, 1\}$, $F_z(t) := \mathbb{P}(s(X, Y) \leq t | Y \in \mathcal{Y}_z(X))$.*

Next, let us state the assumptions that will be used in our theorem.

Assumption 1. *For small $\lambda \geq 0$, the prediction set $\mathcal{C}_\lambda(X)$ is based on the statistical quantile q_λ of the CDF of $s_\lambda(X, Y)$. That is, q_λ obeys $\mathbb{P}(s_\lambda(X, Y) \leq q_\lambda) = 1 - \alpha$.*

Assumption 2. *For $z \in \{0, 1\}$, the CDF $F_z(t)$ is absolutely continuous, so $f_z(t) = F_z'(t)$ is well-defined.*

Assumption 3. *For $z \in \{0, 1\}$, the "size-biased" quasi-CDF $\tilde{F}_z(t) := \frac{1}{\overline{n}_z} \mathbb{E}[n_z(X)\hat{F}_z^X(t)]$ is absolutely continuous, so $\tilde{f}_z(t) = \tilde{F}_z'(t)$ is well-defined.*

Assumptions 1-3 are required for making the analysis tractable, ensuring that $\mathbb{E}[|\mathcal{C}_\lambda(X)|]$ is differentiable with respect to λ, and sparing cumbersome analysis of the effect of finite calibration sets on inclusion of a label in the predictions sets. Note that Assumption 1 essentially reflects having a large calibration set. Now we present a theorem that characterizes the effect of the penalty with small λ on the efficiency.

Theorem 4.5. *Consider Definition 4.4. Under Assumptions 1-3, we have*

$$\text{sign}\left(\frac{\mathrm{d}}{\mathrm{d}\lambda}\mathbb{E}[|\mathcal{C}_\lambda(X)|]\Big|_{\lambda=0}\right) = \text{sign}\left(ap_1\overline{n}_0 - bp_0\overline{n}_1\right),$$

(3)

where $a := \tilde{f}_0(q_0)f_1(q_0)$ and $b := \tilde{f}_1(q_0)f_0(q_0)$.

---

[1]We name the object $\hat{F}_z^x(t)$ "quasi-CDF" because it is not based on any random variable (such as $Y | X = x$) or its realization, but rather on the deterministic set $\mathcal{Y}_z(x)$.

Proof. See Supp. Mat. A.1. The proof sketch is as follows. We establish an expression for the score function CDF, $F_\lambda(t) := \mathbb{P}(s_\lambda(X, Y) \leq t)$ in terms of the conditional CDFs, $F_0(t)$ and $F_1(t)$. By Assumption 1, we have $F_\lambda(q_\lambda) = 1 - \alpha$, on which we apply implicit differentiation and establish an expression for $\frac{dq_\lambda}{d\lambda}$. Based on the definitions we express $\mathbb{E}[|\mathcal{C}_\lambda(X)|]$ using the "size-biased" quasi-CDF. Differentiating it and substituting $\frac{dq_\lambda}{d\lambda}$ at $\lambda = 0$ leads to the advertised result.

$\square$

Discussion. Let us start by assuming that $a \approx b$. In this case, the theorem shows that the sign of $\frac{d}{d\lambda}\mathbb{E}[|\mathcal{C}_\lambda(X)|]\big|_{\lambda=0}$ (where a negative value means that $\lambda \approx 0_+$ reduces $\mathbb{E}[|\mathcal{C}_\lambda(X)|]$) equals the sign of the difference between:

- $p_1 \times \overline{n}_0$: The probability of having the true label out of the group of the predicted class $\times$ the average number of classes in the group of the predicted class.
- $p_0 \times \overline{n}_1$: The probability of having the true label in the group of the predicted class $\times$ the average number of classes out of the group of the predicted class.

We can expect that $p_1\overline{n}_0 \ll p_0\overline{n}_1$ in most practical cases, since typically the number of classes in a group is much smaller than outside a group, i.e., $\overline{n}_0 \ll \overline{n}_1$, and modern classifiers are quite powerful so p_0 is not small. Therefore, if $a \approx b$ or even if b is not much smaller than a, then $\text{sign}(ap_1\overline{n}_0 - bp_0\overline{n}_1) < 0$. By Theorem 4.5, this implies that penalizing the score with small λ will reduce $\mathbb{E}[|\mathcal{C}_\lambda(X)|]$.

Let us discuss the relation between a and b. For simplification, assume that the C classes are partitioned to G groups of equal size K. In this case, we have constants $n_0(X) = K$ and $n_1(X) = (G-1)K$. So, $\overline{n}_0 = K$ and $\overline{n}_1 = (G-1)K$, as well. Recalling the definition of $\tilde{F}_z(t)$ in Assumption 3, we have

$$\tilde{F}_z(t) = \mathbb{E}[\hat{F}_z^X(t)] = \frac{1}{\overline{n}_z}\mathbb{E}\left[\sum_{y \in \mathcal{Y}_z(X)} \mathbb{I}\{s(X, y) \leq t\}\right].$$

Define $p_z(x) := \mathbb{P}(Y \in \mathcal{Y}_z(x)|X = x)$ and $F_z^x(t) := \mathbb{P}(s(x, Y) \leq t|Y \in \mathcal{Y}_z(x), X = x)$. Observe that

$$F_z^x(t) = \frac{\mathbb{P}(s(x, Y) \leq t, Y \in \mathcal{Y}_z(x)|X = x)}{\mathbb{P}(Y \in \mathcal{Y}_z(x)|X = x)}$$
$$= \frac{\sum_{y \in \mathcal{Y}_z(x)} \mathbb{P}(Y = y|X = x)\mathbb{I}\{s(x, y) \leq t\}}{p_z(x)}.$$

Using the relation (see derivation in Supp. Mat. A.2):

$$F_z(t) = \frac{1}{p_z}\mathbb{E}[p_z(X)F_z^X(t)] \tag{4}$$

and substituting in it the expression derived above for $F_z^x(t)$, we get

$$F_z(t) = \frac{1}{p_z}\mathbb{E}[p_z(X)F_z^X(t)]$$
$$= \frac{1}{p_z}\mathbb{E}\left[\sum_{y \in \mathcal{Y}_z(X)} \mathbb{P}(Y = y|X)\mathbb{I}\{s(X, y) \leq t\}\right].$$

Thus, if, per $X = x$, the labels $Y \in \mathcal{Y}_z(x)$ are distributed uniformly, then the factor that multiplies $\mathbb{I}\{s(X, y) \leq t\}$ is constant, and therefore $\tilde{F}_z(t) = F_z(t)$. This gives exact $a = b$ (recall their definitions in Theorem 4.5), so the above arguments hold for having $\text{sign}(ap_1\overline{n}_0 - bp_0\overline{n}_1) < 0$. The fact that the theory includes integration over X and considers the densities only at q_0, together with the empirical fact that $p_1\overline{n}_0 \ll p_0\overline{n}_1$, teach us that there are many cases where $\text{sign}(ap_1\overline{n}_0 - bp_0\overline{n}_1) < 0$ even for non uniform conditional label distributions.

5. Extension to Model-Specific Class Similarity

The original motivation for the penalized score in equation 2 came from considering the potential preference of the user to reduce the number of "semantically far" classes in the prediction set. However, Theorem 4.5 reveals that, perhaps surprisingly, the proposed penalty has a beneficial effect on the prediction set size for any score function, provided that the penalty parameter λ is sufficiently small and $p_1\overline{n}_0 \ll p_0\overline{n}_1$ (omitting the effect of a and b in equation 3).

This result actually tells us that, in terms of efficiency, we can gain more from partitions into groups that are as small as possible (low $\overline{n}_0$ and high $\overline{n}_1$), as long as the probability of making out-of-group mistakes ($p_1 = 1 - p_0$) is kept low. Nothing in this result requires a human-related semantic similarity between classes within a group. This motivates us to propose a *model-specific* extension of the method. Specifically, given a pretrained classifier, we suggest basing the penalty on the class similarity *perceived by the model*. An important advantage of this extension, which focuses on boosting efficiency rather than group-related metrics, is that it eliminates the need for a human-made semantic partition, which may not be available for some datasets.

For a given classifier, the proposed extension requires computing a $C \times C$ class similarity matrix, which we denote by M (recall that C denotes the number of classes). The (c, c') entry in M should reflect the similarity between class c and class c', as perceived by the model. Similarity metrics are typically continuous, e.g., inner products and kernels. Binarization of such metrics will require tuning a threshold parameter. Hence, we propose to diverge slightly from the method in Section 4 by allowing the similarity metric to be "soft", which also adds more flexibility to the method. For $M_{c,c'} \in \mathbb{R}$, upper bounded by 1 as the maximum level of

similarity, we define the soft model-specific penalty function:

$$d^{MS}(y, y') := 1 - M_{y,y'}. \qquad (5)$$

Substituting this penalty in equation 2 in lieu of the model-agnostic d, gives

$$s_\lambda^{MS}(x, y) := s(x, y) + \lambda d^{MS}(y, \hat{y}(x)), \qquad (6)$$

where $\lambda > 0$ is a parameter.

Determining model-specific class similarity. There exist multiple potential strategies for constructing a class similarity matrix M given a model. Here, we propose one that consistently improves the efficiency results in our experiments. Future research may attempt to optimize this choice. We assume access to the labeled training samples. The last layer of a deep neural network-based classifier $f(x) \in \mathbb{R}^C$, before the softmax operation, can be typically expressed as: $f(x) = W h_\theta(x) + b$, where $h_\theta(\cdot) : \mathcal{X} \to \mathbb{R}^p$ (with $p \geq C$) is the deepest feature mapping that is composed of all the hidden layers (with learnable parameters θ), and $W \in \mathbb{R}^{C \times p}$ and $b \in \mathbb{R}^C$ are the weights and bias of the last classification layer. We determine the class similarity according to a similarity function (or kernel) between the means of different classes in the deepest feature space. This strategy is motivated by recent work on the neural collapse phenomenon [16], where the within-class samples of well-trained classifiers concentrate around their class mean in feature space, while inter-class means are well separated yet empirically still preserve relations that generalize to test data [20, 25]. Therefore, examining the relation between class means in feature space yields small effective groups without compromising on group-wise accuracy.

Denote by $\{x_{c,i}\}$, $i \in [n_c]$, the training samples associated with class $c \in [C]$. Compute the class means and the global mean of the features:

$$\overline{h}_c = \frac{1}{n_c} \sum_{i=1}^{n_c} h_\theta(x_{c,i}), \quad c \in [C]. \qquad \overline{h}_G = \frac{1}{C} \sum_{c=1}^{C} \overline{h}_c.$$

We then set the entry $M_{c,c'}$ in the class similarity matrix M using the cosine similarity of the centered class means:

$$M_{c,c'} = \frac{\langle \overline{h}_c - \overline{h}_G, \overline{h}_{c'} - \overline{h}_G \rangle}{\|\overline{h}_c - \overline{h}_G\|\|\overline{h}_{c'} - \overline{h}_G\|}.$$

6. Experiments

Datasets and models. We conduct experiments on three image classification benchmarks: CIFAR-100 [11], Living-17 from the BREEDS suite [19], and Mini-ImageNet [21], a subset of ImageNet [5] with 100 classes. Note that CIFAR-100 and Living-17 have official semantic superclass structures, i.e., partitions of the classes into coarse classes. Specifically, CIFAR-100 has 20 superclasses (e.g., aquatic

mammals, fish, flowers, etc.), where each one groups 5 classes (e.g., beaver, dolphin, otter, seal, and whale are grouped under aquatic mammals). Similarly, Living-17 has 17 superclasses, where each one groups 4 classes. We use ResNet50 [8] as the classifier model. For CIFAR-100 we use ResNet34 as well. Details on the training of the models are provided in Supp. Mat. B.1. We split the validation sets of the datasets to 20% calibration and 80% test.

CP score functions. We consider three prominent conformal score functions $s(x, y)$: (1) LAC [18], defined as one minus the classifier's softmax value at index y; (2) RAPS [2], based on cumulating softmax entries up to the rank of y, like APS [17], but includes a regularization term that yields smaller prediction sets; and (3) SAPS [10], penalizes the maximal softmax entry according to the rank of y. Detailed definitions of these scores are provided in Supp. Mat. B.2. We conduct experiments using target coverage levels of $\alpha = \{0.05, 0.1\}$, as common in the literature.

Details of the CP methods evaluated. For each score function, we evaluate the following versions.

- Standard: The CP algorithm with the original score function and no modifications.
- Clustered [6]: The algorithm extends and improves the efficiency of class-wise Mondrian CP [22] (which applies CP separately to each class) by grouping classes into M clusters based on the similarity of score distributions, and applying CP on each cluster.
  The algorithm has two parameters: γ, which controls the proportion of data used for clustering, and M, the number of clusters. We set $\gamma = 0.2$ to match the proportion used in our methods. M is chosen following [6]. Further details can be found in Appendix B.4 of their paper.
- AIR (Accumulating Inference Rule): Inspired by the *Climbing Inference Rule* [7], which climbs the hierarchy from a predicted leaf node to its parent until reaching a conformalized threshold that guarantees coverage. The exact approach of [7] does not suit the two-level superclass structure of CIFAR-100 and Living-17, as it often leads to the inclusion of all classes. To address this, *we develop an improved variant*. Instead of climbing to the parent, it accumulates mass onto the next superclass with the highest probability, effectively applying conformal prediction at the superclass level rather than the class level.
- MA-CS (Model-Agnostic Class-Similarity): The standard CP algorithm augmented with our binary regularization term, as described in Section 4.
  To select the regularization parameter λ, we split the calibration set into two equal size sets: $\hat{q}$-calibration (used to compute $\hat{q}$), and λ-evaluation (used to evaluate performance for different λ values). We then iterate over a predefined set of λ values and choose the one that achieves the smallest set size on the λ-evaluation set.

Table 1. Performance comparison of various CP methods with $\alpha = 0.05$.

Method	#Superclasses ↓			Size ↓			
	CIFAR100, RN50	CIFAR100, RN34	L17, RN50	m-ImageNet, RN50	CIFAR100, RN50	CIFAR100, RN34	L17, RN50
LAC							
Standard	2.27 (±0.276)	2.41 (±0.274)	1.26 (±0.068)	4.73 (±0.767)	3.68 (±0.759)	3.82 (±0.707)	1.77 (±0.205)
Clustered	2.28 (±0.248)	2.34 (±0.200)	1.24 (±0.035)	4.50 (±0.823)	3.70 (±0.676)	3.62 (±0.485)	1.69 (±0.101)
AIR	**1.36** (±0.097)	**1.43** (±0.091)	**1.16** (±0.040)	N/A	6.80 (±0.101)	7.15 (±0.089)	5.80 (±0.061)
MA-CS	1.85 (±0.183)	1.92 (±0.108)	1.19 (±0.068)	N/A	3.17 (±0.424)	3.51 (±0.749)	1.71 (±0.183)
MS-CS	1.83 (±0.137)	1.87 (±0.126)	1.19 (±0.058)	**3.82** (±0.696)	**2.92** (±0.339)	**2.94** (±0.339)	**1.70** (±0.156)
RAPS							
Standard	2.49 (±0.145)	3.40 (±0.112)	1.35 (±0.052)	8.67 (±2.398)	3.83 (±0.276)	5.79 (±0.223)	1.98 (±0.167)
Clustered	2.42 (±0.103)	3.32 (±0.115)	1.33 (±0.027)	8.19 (±2.224)	3.67 (±0.200)	5.62 (±0.232)	1.90 (±0.090)
AIR	**1.95** (±0.077)	3.03 (±0.085)	**1.20** (±0.026)	N/A	9.75 (±0.121)	15.15 (±0.095)	6.00 (±0.051)
MA-CS	2.01 (±0.160)	2.29 (±0.250)	1.23 (±0.081)	N/A	3.50 (±0.305)	4.52 (±0.501)	1.97 (±0.295)
MS-CS	**1.95** (±0.122)	**2.22** (±0.182)	1.24 (±0.050)	**7.35** (±2.495)	**3.17** (±0.265)	**3.79** (±0.387)	**1.81** (±0.222)
SAPS							
Standard	2.33 (±0.242)	2.39 (±0.17)	1.32 (±0.048)	5.93 (±1.480)	3.45 (±0.458)	3.57 (±0.342)	1.94 (±0.164)
Clustered	2.55 (±0.293)	2.62 (±0.276)	1.31 (±0.045)	8.03 (±2.173)	3.86 (±0.547)	4.02 (±0.521)	2.01 (±0.172)
AIR	**1.51** (±0.163)	**1.59** (±0.124)	**1.11** (±0.032)	N/A	7.55 (±0.324)	7.95 (±0.274)	5.55 (±0.062)
MA-CS	1.88 (±0.286)	1.93 (±0.162)	1.26 (±0.033)	N/A	**3.14** (±0.464)	**3.32** (±0.271)	1.94 (±0.147)
MS-CS	1.97 (±0.187)	2.14 (±0.175)	1.24 (±0.035)	**4.7** (±1.026)	**3.14** (±0.361)	**3.32** (±0.371)	**1.87** (±0.146)

- MS-CS (Model-Specific Class-Similarity): The standard CP algorithm combined with our regularization term based on the model-specific similarity matrix, as detailed in Section 5. The regularization parameter λ is set using the same procedure as in MA-CS.

Note that AIR and our MA-CS cannot be applied for Mini-ImageNet, which lacks a pre-specified superclass structure. On the other hand, our MS-CS is still applicable.

Evaluation metrics. The evaluation metrics that we use are the average prediction set size, and for CIFAR-100 and Living-17 also the average number of superclasses in the prediction set. Note that for these metrics: *the lower the better*. The metrics are computed over the test set and we report their means and standard deviations based on 100 trials (random splits of 20% calibration set and 80% test set). We also compute the marginal coverage. The definitions of the metrics are stated in Supp. Mat. B.3.

6.1. Results

We begin with reporting the top-1 accuracy of each of the four dataset-model pairs: ResNet50 on Mini-ImageNet: 80.38%; ResNet50 on CIFAR-100: 80.93%; ResNet34 on CIFAR-100: 78.92%; ResNet50 on Living-17: 84.68%.

In Tables 3 and 4 in the supplementary, we report the marginal coverage of our MA-CS and MS-CS methods. The pre-specified coverage level is preserved. As expected, our proposed regularization does not affect this property, which is consistent with the CP theoretical guarantee. In the supplementary we report the marginal coverage of the other methods, which also satisfy the specified level.

In Tables 1 and 2 we report the results for the average prediction set size and, when relevant, the average number of superclasses in the prediction set for coverage levels of {0.05, 0.1} respectively. Both tables contain similar findings. Let us discuss the results of Table 1.

Comparison between our methods and Standard/Clustered. Excluding AIR (discussed separately), our methods—MA-CS and MS-CS—consistently achieve the best performance on both metrics across all dataset–model pairs and all CP methods. For example, on CIFAR100–ResNet34 with RAPS score, MA-CS and MS-CS obtain average set size of 4.52 and 3.79, compared to 5.79 and 5.62 for Standard and Clustered, representing a reduction of more than 30%. Similarly, they achieve #Superclasses values of 2.29 and 2.22, whereas Standard and Clustered yield 3.40 and 3.32, corresponding to reductions of approximately 33%.

Comparison between our methods and AIR. For the #Superclasses metric, performance varies across score functions and AIR often achieves lower values. For example, on CIFAR100–ResNet50 with the SAPS score, MA-CS and MS-CS achieve #Superclasses values of 1.88 and 1.97, compared to 1.51 for AIR.

Yet, importantly, for the average size metric, our methods consistently and significantly outperform AIR across all settings. For instance, on CIFAR100-ResNet50 with the RAPS score, MA-CS and MS-CS achieve values of 4.52 and 3.79, compared to 15.15 for AIR, corresponding to a substantial reduction of approximately 75%. Similar reductions are observed throughout the remaining results.

Comparison between MA-CS and MS-CS. Although the two methods achieve similar overall performance, MS is slightly better in most settings. The improvement in the prediction set size can be attributed to the use of smaller groups and the higher flexibility of MS, which leverages model-specific information and "soft" similarity values. Interestingly, for #Superclasses the results are similar to those of MA, despite the distances between classes being derived directly from the model. This may be explained by the overall smaller sets of our MS variant.

Table 2. Performance comparison of various CP methods with $\alpha = 0.1$.

	#Superclasses ↓			Size ↓			
Method	CIFAR100, RN50	CIFAR100, RN34	L17, RN50	m-ImageNet, RN50	CIFAR100, RN50	CIFAR100, RN34	L17, RN50
LAC							
Standard	1.37 (±0.046)	1.44 (±0.051)	1.07 (±0.023)	1.79 (±0.130)	1.62 (±0.084)	1.75 (±0.091)	1.21 (±0.064)
Clustered	1.48 (±0.144)	1.53 (±0.128)	1.09 (±0.036)	2.18 (±0.379)	1.82 (±0.267)	1.90 (±0.221)	1.27 (±0.083)
AIR	**1.02** (±0.097)	**1.09** (±0.091)	1.06 (±0.040)	N/A	5.10 (±0.101)	5.45 (±0.089)	5.30 (±0.061)
MA-CS	1.24 (±0.063)	1.34 (±0.065)	**1.04** (±0.018)	N/A	1.54 (±0.127)	1.70 (±0.120)	1.19 (±0.037)
MS-CS	1.25 (±0.053)	1.32 (±0.072)	1.05 (±0.015)	**1.69** (±0.158)	**1.53** (±0.092)	**1.65** (±0.138)	**1.18** (±0.042)
RAPS							
Standard	1.92 (±0.053)	2.69 (±0.062)	1.19 (±0.019)	3.79 (±0.142)	2.70 (±0.102)	4.33 (±0.125)	1.51 (±0.049)
Clustered	1.91 (±0.087)	2.64 (±0.108)	1.20 (±0.098)	4.28 (±0.661)	2.69 (±0.166)	4.22 (±0.222)	1.54 (±0.122)
AIR	1.52 (±0.077)	1.63 (±0.085)	1.10 (±0.026)	N/A	7.60 (±0.121)	8.15 (±0.095)	5.50 (±0.051)
MA-CS	**1.34** (±0.099)	**1.45** (±0.100)	**1.03** (±0.032)	N/A	2.10 (±0.177)	2.60 (±0.165)	1.38 (±0.053)
MS-CS	**1.34** (±0.085)	1.49 (±0.080)	1.07 (±0.020)	**2.05** (±0.203)	**1.89** (±0.160)	**2.18** (±0.174)	**1.28** (±0.056)
SAPS							
Standard	1.48 (±0.110)	1.57 (±0.096)	1.10 (±0.017)	2.16 (±0.395)	1.83 (±0.204)	1.97 (±0.186)	1.29 (±0.044)
Clustered	1.60 (±0.265)	1.73 (±0.299)	1.20 (±0.224)	2.96 (±0.760)	1.99 (±0.336)	2.18 (±0.406)	1.49 (±0.236)
AIR	**1.16** (±0.039)	**1.10** (±0.023)	**1.02** (±0.017)	N/A	5.80 (±0.207)	5.50 (±0.155)	4.03 (±0.145)
MA-CS	1.26 (±0.044)	1.42 (±0.063)	1.06 (±0.012)	N/A	1.74 (±0.140)	1.89 (±0.163)	1.27 (±0.062)
MS-CS	1.36 (±0.084)	1.39 (±0.059)	1.07 (±0.013)	**1.95** (±0.239)	**1.71** (±0.172)	**1.81** (±0.136)	**1.24** (±0.049)

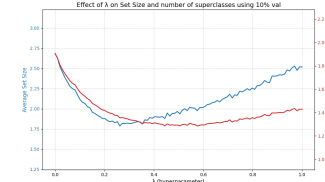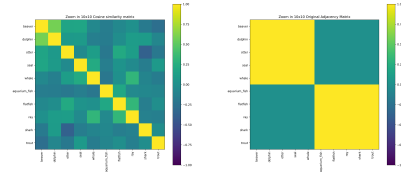## 6.2. The effect of λ on the metrics

In this section, we examine how the penalty coefficient λ influences both the #Superclasses and the average prediction-set size. In Figure 2, we present both metrics for different values of λ. In order to emphasize practical usage we used only 10% of the data for calibration and another 10% for validation. As expected, for a large range of λ the #Superclasses decreases as λ increases, reflecting the intended effect of the penalty. The slight increase starting from a very large (impractical) value of λ can be explained by a decrease in number of samples with empty prediction sets. Namely, even for samples where the minimal score across labels is quite large, due to overly large λ the CP threshold becomes large enough to upper bound the minimal score.

As for the average set size, observe that it initially decreases for small values of λ, aligned with Theorem 4.5. Then, after reaching a minimum, the metric increases with λ. These observations suggest that there exists a regime of λ in which both metrics exhibit improvement, underscoring the practical value of appropriately tuning the regularization strength. In Figure 2, we observe that for $\lambda \in (0, 0.28]$ both metrics improve. At $\lambda = 0.28$, the method achieves a substantial reduction of approximately 33% in the average prediction-set size and 25% in the #Superclasses. Notably, we demonstrate that this tuning process for λ can be conducted using only 20% of the data, requires just a single trial, and can be completed within a matter of minutes.

In the supplementary we further show robustness of a class-conditional coverage metric to changes in λ.

6.3. Model-perceived class similarity

In this part, we show the similarity between classes as perceived by the model. For CIFAR100-ResNet50 we present in Figure 3 the top-left 10×10 block of the similarity matrix M (defined in section 5). The associated model-agnostic similarity is depicted as well. The complete matrices are

Figure 2. The effect of λ on the average set size (blue) and number of superclasses (red) for CIFAR-100, ResNet50 and RAPS score.

Figure 3. Comparison of zoomed 10×10 regions of the model specific (left) and model agnostic (right) similarity matrices.

provided in the supplementary.

To further highlight the advantage of the model-perceived class similarity, we also compare the performance of the MS-CS matrix against the identity matrix $M = I$, which equally punishes all classes except the prediction. The experiments in the supplementary, demonstrating the superiority of MS-CS similarity matrix over this matrix, suggesting using the learned embeddings from the model itself is highly valuable.

7. Conclusion

In this paper, we proposed a class-similarity-based regularization approach that can be applied to any CP score function and reduces *both* the number of groups *and* the overall size of the prediction sets. We backed our model-agnostic variant with comprehensive theory, which also motivated us to extend it to a novel model-specific approach. Importantly, the latter reduces the prediction set size even further and does not require any known class structure, making it a widely applicable tool in the CP toolbox.

Acknowledgments

References

[1] Anastasios N Angelopoulos and Stephen Bates. A gentle introduction to conformal prediction and distribution-free uncertainty quantification. *arXiv preprint arXiv:2107.07511*, 2021. 3

[2] Anastasios Nikolas Angelopoulos, Stephen Bates, Michael Jordan, and Jitendra Malik. Uncertainty sets for image classifiers using conformal prediction. In *International Conference on Learning Representations*, 2021. 1, 2, 6

[3] Konstantina Bairaktari, Jiayun Wu, and Zhiwei Steven Wu. Kandinsky conformal prediction: Beyond class- and covariate-conditional coverage. *arXiv preprint arXiv:2502.17264*, 2025. 2

[4] Lahav Dabah and Tom Tirer. On temperature scaling and conformal prediction of deep classifiers. In *Forty-second International Conference on Machine Learning*, 2025. 1

[5] Jia Deng, Wei Dong, Richard Socher, Li-Jia Li, Kai Li, and Li Fei-Fei. Imagenet: A large-scale hierarchical image database. In *2009 IEEE conference on computer vision and pattern recognition*, pages 248–255. Ieee, 2009. 6

[6] Tiffany Ding, Anastasios Angelopoulos, Stephen Bates, Michael Jordan, and Ryan J Tibshirani. Class-conditional conformal prediction with many classes. *Advances in Neural Information Processing Systems*, 36, 2023. 2, 6

[7] Shani Goren, Ido Galil, and Ran El-Yaniv. Hierarchical selective classification. *Advances in Neural Information Processing Systems*, 37:111047–111073, 2024. 2, 6

[8] Kaiming He, Xiangyu Zhang, Shaoqing Ren, and Jian Sun. Deep residual learning for image recognition. In *Proceedings of the IEEE conference on computer vision and pattern recognition*, pages 770–778, 2016. 6

[9] Floris den Hengst, Inès Blin, Majid Mohammadi, Syed Ihtesham Hussain Shah, and Taraneh Younesian. Hierarchical conformal classification. *arXiv preprint arXiv:2508.13288*, 2025. 2

[10] Jianguo Huang, Huajun Xi, Linjun Zhang, Huaxiu Yao, Yue Qiu, and Hongxin Wei. Conformal prediction for deep classifier via label ranking. In *International Conference on Machine Learning*, pages 20331–20347. PMLR, 2024. 1, 2, 6

[11] Alex Krizhevsky, Geoffrey Hinton, et al. Learning multiple layers of features from tiny images. 2009. 6

[12] Benjamin Lambert, Florence Forbes, Senan Doyle, Harmonie Dehaene, and Michel Dojat. Trustworthy clinical AI solutions: A unified review of uncertainty quantification in deep learning models for medical image analysis. *Artif. Intell. Medicine*, 150:102830, 2024. 1

[13] Lars Lindemann, Yiqi Zhao, Xinyi Yu, George J Pappas, and Jyotirmoy V Deshmukh. Formal verification and control with conformal prediction. *arXiv preprint arXiv:2409.00536*, 2024. 1

[14] Thomas Mortier, Alireza Javanmardi, Yusuf Sale, Eyke Hüllermeier, and Willem Waegeman. Conformal prediction in hierarchical classification. *arXiv preprint arXiv:2501.19038*, 2025. 2

[15] Harris Papadopoulos, Kostas Proedrou, Volodya Vovk, and Alex Gammerman. Inductive confidence machines for regression. In *Machine Learning: ECML 2002: 13th European Conference on Machine Learning Helsinki, Finland, August 19–23, 2002 Proceedings 13*, pages 345–356. Springer, 2002. 3

[16] Vardan Papyan, XY Han, and David L Donoho. Prevalence of neural collapse during the terminal phase of deep learning training. *Proceedings of the National Academy of Sciences*, 117(40):24652–24663, 2020. 6

[17] Yaniv Romano, Matteo Sesia, and Emmanuel Candes. Classification with valid and adaptive coverage. *Advances in Neural Information Processing Systems*, 33:3581–3591, 2020. 2, 6

[18] Mauricio Sadinle, Jing Lei, and Larry Wasserman. Least ambiguous set-valued classifiers with bounded error levels. *Journal of the American Statistical Association*, 114(525): 223–234, 2019. 1, 2, 6

[19] Shibani Santurkar, Dimitris Tsipras, and Aleksander Madry. Breeds: Benchmarks for subpopulation shift. *arXiv preprint arXiv:2008.04859*, 2020. 6

[20] Tom Tirer, Haoxiang Huang, and Jonathan Niles-Weed. Perturbation analysis of neural collapse. In *International Conference on Machine Learning*, pages 34301–34329. PMLR, 2023. 6

[21] Oriol Vinyals, Charles Blundell, Timothy Lillicrap, Daan Wierstra, et al. Matching networks for one shot learning. *Advances in neural information processing systems*, 29, 2016. 6

[22] Vladimir Vovk. Conditional validity of inductive conformal predictors. In *Asian conference on machine learning*, pages 475–490. PMLR, 2012. 2, 6

[23] Volodya Vovk, Alexander Gammerman, and Craig Saunders. Machine-learning applications of algorithmic randomness. In *Proceedings of the Sixteenth International Conference on Machine Learning*, pages 444–453, 1999. 1, 3

[24] Vladimir Vovk, Alexander Gammerman, and Glenn Shafer. *Algorithmic learning in a random world*. Springer, 2005. 1, 3

[25] Yongyi Yang, Jacob Steinhardt, and Wei Hu. Are neurons actually collapsed? on the fine-grained structure in neural representations. In *International Conference on Machine Learning*, pages 39453–39487. PMLR, 2023. 6

[26] Botong Zhang, Shuo Li, and Osbert Bastani. Conformal structured prediction. *arXiv preprint arXiv:2410.06296*, 2024. 2

A. Proofs and Additional Derivations

A.1. Proof of Theorem 4.5

From the definition of $s_\lambda(x, y)$, for any fixed x, the size of the penalized conformal set can be written as

$$|\mathcal{C}_\lambda(x)| = \sum_{y \in \mathcal{Y}_0(x)} \mathbb{I}\{s(x, y) \le q_\lambda\} + \sum_{y \in \mathcal{Y}_1(x)} \mathbb{I}\{s(x, y) \le q_\lambda - \lambda\}$$

$$= n_0(x)\hat{F}_0^x(q_\lambda) + n_1(x)\hat{F}_1^x(q_\lambda - \lambda),$$

where in the first equation we used q_λ due to Assumption 1, and in the second equation we used the definition of $\hat{F}_z^x(t)$. By the law of total expectation,

$$\mathbb{E}[|\mathcal{C}_\lambda(X)|] = \mathbb{E}[n_0(X)\hat{F}_0^X(q_\lambda)] + \mathbb{E}[n_1(X)\hat{F}_1^X(q_\lambda - \lambda)].$$

Using the definition of $\tilde{F}_z(t)$ in Assumption 3, we get

$$\mathbb{E}[|\mathcal{C}_\lambda(X)|] = \bar{n}_0 \, \tilde{F}_0(q_\lambda) + \bar{n}_1 \, \tilde{F}_1(q_\lambda - \lambda). \tag{7}$$

Next, recall that q_λ is defined as the $(1 - \alpha)$–quantile of the CDF $F_\lambda(t) := \mathbb{P}(s_\lambda(X, Y) \le t)$. Namely, $F_\lambda(q_\lambda) = 1 - \alpha$. Observe that

$$F_\lambda(t) = \mathbb{P}(Y \in \mathcal{Y}_0(x))F_0(t) + \mathbb{P}(Y \in \mathcal{Y}_1(x))F_1(t - \lambda)$$

$$= p_0 F_0(t) + p_1 F_1(t - \lambda).$$

Applying implicit differentiation, by differentiating both sides of $F_\lambda(q_\lambda) = 1 - \alpha$ with respect to λ (valid due to Assumption 2), we get

$$\frac{\partial F_\lambda}{\partial \lambda}(q_\lambda) + \frac{\partial F_\lambda}{\partial t}(q_\lambda) \frac{dq_\lambda}{d\lambda} = 0.$$

Since

$$\frac{\partial F_\lambda}{\partial t}(t) = p_0 f_0(t) + p_1 f_1(t - \lambda), \quad \frac{\partial F_\lambda}{\partial \lambda}(t) = -p_1 f_1(t - \lambda),$$

we obtain

$$\frac{dq_\lambda}{d\lambda} = \frac{p_1 f_1(q_\lambda - \lambda)}{p_0 f_0(q_\lambda) + p_1 f_1(q_\lambda - \lambda)}.$$

At $\lambda = 0$ (with $q = q_0$),

$$\left. \frac{dq_\lambda}{d\lambda} \right|_{\lambda=0} = \frac{p_1 f_1(q)}{p_0 f_0(q) + p_1 f_1(q)}. \tag{8}$$

Now, let us differentiate equation 7 with respect to λ (valid due to Assumption 3):

$$\frac{d}{d\lambda} \mathbb{E}[|\mathcal{C}_\lambda(X)|] = \bar{n}_0 \tilde{f}_0(q_\lambda) \frac{dq_\lambda}{d\lambda} + \bar{n}_1 \tilde{f}_1(q_\lambda - \lambda) \left(\frac{dq_\lambda}{d\lambda} - 1 \right).$$

Evaluating at $\lambda = 0$ and substituting equation 8,

$$\left. \frac{d}{d\lambda} \mathbb{E}[|\mathcal{C}_\lambda(X)|] \right|_{\lambda=0} = \bar{n}_0 \tilde{f}_0(q) \frac{p_1 f_1(q)}{p_0 f_0(q) + p_1 f_1(q)} + \bar{n}_1 \tilde{f}_1(q) \left(\frac{p_1 f_1(q)}{p_0 f_0(q) + p_1 f_1(q)} - 1 \right)$$

$$= \frac{1}{p_0 f_0(q) + p_1 f_1(q)} \left(\tilde{f}_0(q) f_1(q) \cdot p_1 \bar{n}_0 - \tilde{f}_1(q) f_0(q) \cdot p_0 \bar{n}_1 \right).$$

Since $\dfrac{1}{p_0 f_0(q) + p_1 f_1(q)} > 0$ (strictly positive), we obtain equation 3.

A.2. Derivation of equation 4

To simplify the notation, define the event $A_z = Y \in \mathcal{Y}_z(X)$. We have

$$
\begin{aligned}
F_z(t) &= \mathbb{P}(s(X,Y) \le t | A_z) \\
&= \mathbb{E}_{X,Y|A_z}[\mathbb{I}\{s(X,Y) \le t\}] \\
&= \mathbb{E}_{X|A_z}[\mathbb{E}_{Y|A_z,X}[\mathbb{I}\{s(X,Y) \le t\}]] \\
&= \mathbb{E}_{X|A_z}[\mathbb{P}(s(x,Y) \le t | Y \in \mathcal{Y}_z(X), X)] \\
&= \mathbb{E}_{X|A_z}[F_z^X(t)]
\end{aligned}
$$

Next, using $p_{X|A_z}(x) = \dfrac{\mathbb{P}(A_z|X=x)p_X(x)}{\mathbb{P}(A_z)} = \dfrac{p_z(x)p_X(x)}{p_z}$, we have

$$
\begin{aligned}
F_z(t) &= \int F_z^x(t) p_{X|A_z}(x) dx \\
&= \frac{1}{p_z} \int F_z^x(t) p_z(x) p_X(x) dx \\
&= \frac{1}{p_z} \mathbb{E}[p_z(X) F_z^X(t)].
\end{aligned}
$$

B. Additional Experimental Details

B.1. Training details

For CIFAR-100 models, we use the following: Batch size: 128; Epochs: 100; Cross entropy loss; Optimizer: SGD; Learning rate: 0.1; Momentum 0.9 and weight decay 0.0005.
Similarly, for Living 17 we use: Batch size: 64; Epochs: 15; Cross entropy loss; Optimizer: Adam; Learning rate: 0.0001.
For training details regarding Mini-ImageNet, see the following link:
https://huggingface.co/datasets/timm/mini-ImageNet

B.2. Definitions of the score functions

LAC:

$$s(x, y) := 1 - \hat{\pi}(x, y) \tag{9}$$

RAPS:

$$s(x, y) := \sum_{y'=1}^{C} \hat{\pi}(x, y') \mathbf{1}\{\hat{\pi}(x, y') > \hat{\pi}(x, y)\} + \lambda_{RAPS} \cdot \left(o_x(y) - k_{\text{reg}}\right)^+ + \hat{\pi}(x, y) \cdot u, \tag{10}$$

where

$$o_x(y) = \left|\{ y' \in \mathcal{Y} : \hat{\pi}(x, y') \geq \hat{\pi}(x, y) \}\right|,$$

$(x)^+$ is the positive part of the expression and λ_{RAPS}, k_{reg} are hyperparameters, which we set as in the original RAPS implementation.
SAPS:

$$S(x, y) := \begin{cases} u \cdot \hat{\pi}_{\max}(x, y), & \text{if } o_x(y) = 1 \\ \hat{\pi}_{\max}(x, y) + \left(o_x(y) - 2 + u\right) \cdot \lambda_{SAPS}, & \text{else} \end{cases} \tag{11}$$

where u is a uniform random variable and $\hat{\pi}_{\max}(x, y)$ denotes the maximum softmax. We optimized the hyperparameter λ_{SAPS} per model-dateset pair to a fixed value that minimizes the average set size (the values where roughly around 0.08).

B.3. Definitions of the evaluation metrics

We report metrics over the test set, which we denote by $\{(\mathbf{x}_i^{(test)}, y_i^{(test)})\}_{i=1}^{N_{test}}$, comprising of the samples that were not included in the calibration set. The metrics are as follows.

• *Average set size* – The mean prediction set size of the CP algorithm:

$$\text{Average Size} = \frac{1}{N_{test}} \sum_{i=1}^{N_{test}} |\mathcal{C}(\mathbf{x}_i^{(test)})|.$$

• *Average number of superclasses* - The mean number of distinct superclasses in prediction set of the CP algorithm.

$$\text{Average \#Superclasses} = \frac{1}{N_{test}} \sum_{i=1}^{N_{test}} |\mathcal{G}(\mathbf{x}_i^{(test)})|.$$

where $\mathcal{G}(x) = \{g(y) : y \in \mathcal{C}(x)\}$
• *Marginal coverage* - The coverage rate of the prediction sets of the CP algorithm:

$$\text{Coverage rate} = \frac{1}{N_{test}} \sum_{i=1}^{N_{test}} \mathbf{1}\{y_i \in \mathcal{C}(x_i^{(test)})\}.$$

C. Additional Experiments

C.1. Marginal coverage

In Tables 3, we present the marginal coverage for each of the methods and all the settings for $\alpha = 0.05$. Similarly, in Table 4 we present the marginal coverage for $\alpha = 0.1$. As expected from Theorem 3.1, the marginal coverage holds.

Table 3. Marginal coverage of the CP methods for $\alpha = 0.05$.

	Coverage			
Method	Mini ImageNet	CIFAR100 RN50	CIFAR100 RN34	L17
LAC				
Standard	0.952	0.950	0.952	0.953
Clustered	0.950	0.951	0.950	0.950
AIR	N/A	0.951	0.954	0.948
MA-CS	N/A	0.950	0.951	0.949
MS-CS	0.949	0.950	0.947	0.950
RAPS				
Standard	0.951	0.950	0.951	0.955
Clustered	0.950	0.950	0.951	0.951
AIR	N/A	0.950	0.952	0.951
MA-CS	N/A	0.950	0.949	0.952
MS-CS	0.951	0.948	0.948	0.950
SAPS				
Standard	0.952	0.950	0.951	0.950
Clustered	0.950	0.951	0.949	0.950
AIR	N/A	0.954	0.946	0.950
MA-CS	N/A	0.946	0.943	0.951
MS-CS	0.948	0.946	0.949	0.951

Table 4. Marginal coverage of the CP methods for $\alpha = 0.1$.

	Coverage			
Method	Mini ImageNet	CIFAR100 RN50	CIFAR100 RN34	L17
LAC				
Standard	0.901	0.899	0.902	0.905
Clustered	0.895	0.915	0.919	0.902
AIR	N/A	0.905	0.902	0.901
MA-CS	N/A	0.900	0.895	0.898
MS-CS	0.896	0.897	0.899	0.899
RAPS				
Standard	0.898	0.900	0.903	0.902
Clustered	0.902	0.917	0.913	0.903
AIR	N/A	0.906	0.907	0.904
MA-CS	N/A	0.899	0.899	0.900
MS-CS	0.901	0.898	0.900	0.905
SAPS				
Standard	0.900	0.898	0.904	0.899
Clustered	0.901	0.900	0.900	0.902
AIR	N/A	0.908	0.896	0.900
MA-CS	N/A	0.898	0.900	0.898
MS-CS	0.898	0.900	0.899	0.900

C.2. The effect of our penalty on conditional coverage

First, we define our conditional coverage metric:

Worst class-coverage gap - The highest deviation from the desired 1-α coverage:

$$\text{TopCovGap} = \text{Max}_{y \in [C]} \left| \frac{1}{|I_y|} \sum_{i \in I_y} \mathbf{1} \left\{ y_i^{(\text{test})} \in \mathcal{C} \left(x_i^{(\text{test})} \right) \right\} - (1 - \alpha) \right|,$$

where $I_y = \{i \in [N_{test}] : y_i^{(\text{test})} = y\}$ is the indices of the test examples labeled y.

In Figure 4, we illustrate how the penalty hyperparameter λ influences both the average set size and the conditional coverage. For our experiments, 10% of the data was allocated for calibration and an additional 10% for validation. As λ increases, the average set size initially decreases, reaches a minimum, and then begins to rise again. For conditional coverage, we report the *TopCovGap* metric, which remains relatively stable across the range of λ values.
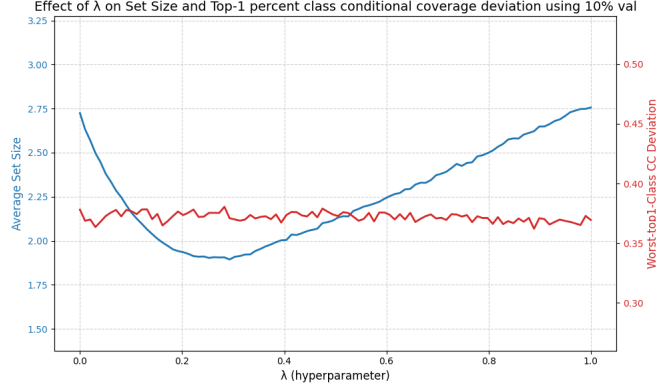

Figure 4. Average set size (blue) and worst class conditional coverage deviation (red) over hyperparamter λ in RAPS method Model Specific with model CIFAR-100 Resnet 50. Average set size is reaching a minimum along with λ while the class conditinal remains stabilized.

Table 5. TopCovGap of the CP methods for $\alpha = 0.05$.

Method	m-ImageNet, RN50	CIFAR100, RN50	CIFAR100, RN34	L17, RN50
		TopCovGap		
LAC				
Standard	0.106	0.101	0.114	0.182
Clustered	0.125	0.102	0.118	0.226
AIR	N/A	0.086	0.123	0.127
MA-CS	N/A	0.111	0.125	0.206
MS-CS	0.128	0.096	0.109	0.168
RAPS				
Standard	0.122	0.078	0.083	0.160
Clustered	0.143	0.099	0.092	0.183
AIR	N/A	0.061	0.093	0.097
MA-CS	N/A	0.099	0.135	0.169
MS-CS	0.136	0.090	0.118	0.160
SAPS				
Standard	0.128	0.106	0.134	0.213
Clustered	0.136	0.091	0.145	0.218
AIR	N/A	0.070	0.099	0.100
MA-CS	N/A	0.118	0.173	0.186
MS-CS	0.144	0.095	0.115	0.219

14

Table 6. TopCovGap of the CP methods for $\alpha = 0.1$.

Method	TopCovGap			
	Mini ImageNet	CIFAR100 RN50	CIFAR100 RN34	L17
LAC				
Standard	0.180	0.194	0.169	0.372
Clustered	0.183	0.186	0.179	0.312
AIR	N/A	0.196	0.211	0.306
MA-CS	N/A	0.143	0.183	0.372
MS-CS	0.183	0.164	0.192	0.346
RAPS				
Standard	0.129	0.139	0.101	0.224
Clustered	0.134	0.149	0.140	0.235
AIR	N/A	0.144	0.120	0.102
MA-CS	N/A	0.131	0.176	0.261
MS-CS	0.163	0.148	0.177	0.277
SAPS				
Standard	0.188	0.156	0.180	0.368
Clustered	0.180	0.175	0.181	0.302
AIR	N/A	0.146	0.251	0.198
MA-CS	N/A	0.135	0.201	0.346
MS-CS	0.197	0.158	0.190	0.273

D. Visualization and Ablation Study of the Model-Specific Class Similarity

D.1. Visualization

In this section, we examine the cosine class similarity, as described in Section 5, using the class similarity matrix M. The image on the left shows the full similarity matrix, in contrast to the 10×10 zoomed-in view presented in the left panel of Figure 3. The right image similarly displays the full, unzoomed version of the model-agnostic superclass association matrix.

(a) Similarity matrix learned by ResNet50 on CIFAR-100.　　　　(b) Original superclass matrix of CIFAR-100.

Figure 5. Comparison of the ResNet50 model-specific similarity matrix and the original superclass matrix of CIFAR-100.

D.2. Ablation study

In this section, we further emphasize the benefits of incorporating model-perceived class similarity. To this end, we compare the performance of our MS-CS matrix, which uses a similarity matrix M detailed in Section 5, with a version that uses a simple identity matrix $M = I$, which is model-agnostic and penalizes all non-predicted classes equally. We refer to this baseline as Model-Agnostic Diagonal (MA-Diag). Tuning the hyperparameter λ for MA-Diag is done exactly as for MA-CS and MS-CS.

Tables 7 and 8 report the resulting number of superclasses and prediction-set sizes across all dataset–model pairs and CP algorithms for $\alpha \in \{0.05, 0.1\}$, respectively. Across all settings and for both evaluation metrics, MA-Diag never outperforms either MA-CS or MS-CS. This demonstrates the clear advantage of accounting for inter-class similarity—whether derived from semantic structure or captured implicitly by the model's learned embeddings. We also note that, unlike our method, the naive MA-Diag does have reduced average prediction set size compared to the standard LAC (cf. Tables 1 and 2).

Table 7. Performance comparison of model agnostic and specific methods with $\alpha = 0.05$.

Method	#Superclasses ↓			Size ↓			
	CIFAR100, RN50	CIFAR100, RN34	L17, RN50	Mini-ImageNet	CIFAR100, RN50	CIFAR100, RN34	L17, RN50
LAC							
MA-CS	1.85 (±0.183)	1.92 (±0.108)	**1.19** (±0.068)	N/A	3.17 (±0.424)	3.51 (±0.749)	1.71 (±0.183)
MS-CS	**1.83** (±0.137)	**1.87** (±0.126)	**1.19** (±0.058)	**3.82** (±0.696)	**2.92** (±0.339)	**2.94** (±0.339)	**1.70** (±0.156)
MA-Diag	2.29 (±0.285)	2.38 (±0.285)	1.26 (±0.059)	4.93 (±1.050)	3.74 (±0.785)	3.74 (±0.724)	1.77 (±0.177)
RAPS							
MA-CS	2.01 (±0.160)	2.29 (±0.250)	**1.23** (±0.081)	N/A	3.50 (±0.305)	4.52 (±0.501)	1.97 (±0.295)
MS-CS	**1.95** (±0.122)	**2.22** (±0.182)	1.24 (±0.050)	**7.35** (±2.495)	**3.17** (±0.265)	**3.79** (±0.387)	**1.81** (±0.222)
MA-Diag	2.40 (±0.144)	3.13 (±0.186)	1.32 (±0.071)	8.63 (±2.256)	3.65 (±0.282)	5.23 (±0.389)	1.87 (±0.236)
SAPS							
MA-CS	**1.88** (±0.286)	**1.93** (±0.162)	1.26 (±0.033)	N/A	**3.14** (±0.464)	**3.32** (±0.271)	1.94 (±0.147)
MS-CS	1.97 (±0.187)	2.14 (±0.175)	**1.24** (±0.035)	**4.7** (±1.026)	**3.14** (±0.361)	**3.32** (±0.371)	**1.87** (±0.146)
MA-Diag	2.29 (±0.203)	2.36 (±0.176)	1.32 (±0.105)	5.61 (±1.441)	3.38 (±0.393)	3.52 (±0.346)	1.99 (±0.357)

Table 8. Performance comparison of model agnostic and specific methods with $\alpha = 0.1$.

Method	#Superclasses ↓			Size ↓			
	CIFAR100, RN50	CIFAR100, RN34	L17, RN50	Mini-ImageNet	CIFAR100, RN50	CIFAR100, RN34	L17, RN50
LAC							
MA-CS	**1.24** (±0.063)	1.34 (±0.065)	**1.04** (±0.018)	N/A	1.54 (±0.127)	1.70 (±0.120)	1.19 (±0.037)
MS-CS	1.25 (±0.053)	**1.32** (±0.072)	1.05 (±0.015)	**1.69** (±0.158)	**1.53** (±0.092)	**1.65** (±0.138)	**1.18** (±0.042)
MA-Diag	1.39 (±0.067)	1.44 (±0.068)	1.08 (±0.040)	1.79 (±0.209)	1.67 (±0.123)	1.74 (±0.121)	1.25 (±0.113)
RAPS							
MA-CS	**1.34** (±0.099)	**1.45** (±0.100)	**1.03** (±0.032)	N/A	2.10 (±0.177)	2.60 (±0.165)	1.38 (±0.053)
MS-CS	**1.34** (±0.085)	1.49 (±0.080)	1.07 (±0.020)	**2.05** (±0.203)	**1.89** (±0.160)	**2.18** (±0.174)	**1.28** (±0.056)
MA-Diag	1.67 (±0.099)	1.99 (±0.115)	1.14 (±0.036)	2.29 (±0.212)	2.19 (±0.199)	2.82 (±0.241)	1.31 (±0.091)
SAPS							
MA-CS	**1.26** (±0.044)	1.42 (±0.063)	**1.06** (±0.012)	N/A	1.74 (±0.140)	1.89 (±0.163)	1.27 (±0.062)
MS-CS	1.36 (±0.084)	**1.39** (±0.059)	1.07 (±0.013)	**1.95** (±0.239)	**1.71** (±0.172)	**1.81** (±0.136)	**1.24** (±0.049)
MA-Diag	1.45 (±0.094)	1.54 (±0.093)	1.1 (±0.034)	2.07 (±0.330)	1.78 (±0.179)	1.92 (±0.182)	1.27 (±0.105)